

Spectral domain nonlinear quantum interferometry with pulsed laser excitationJasleen Kaur , Yu Mukai , Ryo Okamoto , and Shigeki Takeuchi **Department of Electronic Science and Engineering, Kyoto University, Kyotodaigakukatsura, Nishikyo-ku, Kyoto 615-8510, Japan*

(Received 20 August 2023; accepted 22 November 2023; published 22 December 2023)

Nonlinear quantum interferometry is widely used in photonic quantum sensing applications to perform measurements with undetected photons. While continuous wave (cw) lasers are typically used to generate correlated photon pairs, pulsed laser pumping can enhance the generation efficiency for photon pairs and enable time-resolved measurements. However, the finite spectral linewidth of pulsed lasers leads to imperfect frequency correlation between generated photon pairs, which can affect the sensitivity of nonlinear interferometry. In this work, we investigate the effect of the finite linewidth of a pump laser on the visibility of spectral domain interference in a nonlinear quantum interferometer where signal photons are detected using a dispersive spectrometer. The proposed theory quantitatively predicts the visibility as a function of optical path difference for a pump source with arbitrary spectrum. As a demonstration, we construct an experimental setup to obtain quantum interference using both cw and pulsed laser excitations under the same experimental conditions. At large optical path differences, a fine interference fringe pattern with high contrast is observed with cw laser excitation, whereas with pulsed laser pumping, the visibility decreases as the optical path delay increases, and the interference fringes appear almost washed out. Our quantitative analysis is useful for determining appropriate pulsed laser parameters for designing nonlinear interferometers for quantum sensing applications using a dispersive spectrometer.

DOI: [10.1103/PhysRevA.108.063714](https://doi.org/10.1103/PhysRevA.108.063714)**I. INTRODUCTION**

The use of quantum entangled states for sensing is attracting attention [1–5]. One of the uses is the “sensing with undetected photons” [6–8]. By using the quantum interference between the processes of spontaneous parametric down conversion (SPDC) in nonlinear crystals, nonlinear interferometers allow the properties of a sample placed in the probe beam to be extracted by detecting the correlated reference beam [9]. This provides the freedom to choose a detection frequency for which efficient detectors are available. Recently, this technique has been extensively explored in the infrared region to circumvent the need for infrared (IR) sources and detectors, which are inherently inefficient [10], and replace them with mature off-the-shelf, room-temperature operable visible-range technology. Motivated by these advantages, numerous experiments have been reported demonstrating optical coherence tomography (OCT) [11,12], quantum imaging [9], infrared microscopy [13,14], and quantum infrared spectroscopy (QIRS) in the mid-infrared region [15–18] and recently even in the fingerprint region [19,20] by detecting visible light photons via silicon-based detectors.

In the spectral domain nonlinear quantum interferometry, a visible-light interferogram is obtained by detecting signal photons using a dispersive spectrometer [12,21–23]. The spectral domain method offers a faster acquisition time and improved mechanical stability over the time domain technique. Applications such as dispersive-QIRS [21–23] and frequency-domain (FD) OCT [12] have been demonstrated with a nonlinear quantum interferometer using a dispersive spectrometer.

Most of these experiments have been implemented using a continuous wave (cw) laser for pumping. Alternatively, it may be interesting to use pulsed lasers as excitation sources for SPDC processes. One of the reasons is the possibility for the applications of such a system for time-resolved measurements. Another reason is the efficient generation of correlated photons in the transition between the low-gain regime and the high-gain regime [24].

However, unlike cw lasers, the finite spectral width of a pulsed laser leads to imperfect frequency correlation that can reduce the contrast of spectral domain interference and may affect the sensitivity of dispersive QIRS and FD-OCT techniques. As far as we know, to date, the quantitative study of the effect of the finite linewidth of pulsed laser sources on the spectral domain nonlinear quantum interferometry in the low parametric gain (quantum) regime has not been reported.

In the present study, we theoretically and experimentally investigate the effect of the linewidth of pulsed laser excitation in a nonlinear quantum interferometer observed with a dispersive spectrometer. We theoretically predict that with pulsed laser pumping, the visibility of quantum interference at each signal wavelength decreases with increasing optical delay, leading to a reduced contrast of the interference fringe pattern. We verify this prediction by constructing an experimental setup in which the spectral domain quantum interference can be obtained under the same experimental conditions using both cw and pulsed laser sources. While a fine interference fringe pattern with high contrast is observed for cw laser pumping, the contrast decreases and the fringes appear washed out in the case of pulsed laser pumping. Further, we evaluate the quantum interference visibility at each spectral component of the signal photons. For cw laser pumping, the visibility remains almost constant while

*takeuchi@kuee.kyoto-u.ac.jp

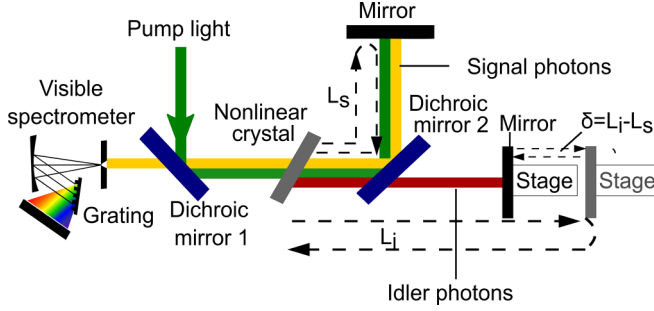


FIG. 1. Schematic of Michelson-type nonlinear quantum interferometer.

varying the path delay; however, a significant reduction in visibility with an increase in path delay is noted while using pulsed laser excitation. These results are in good agreement with the theoretical predictions. This quantitative analysis is important while designing nonlinear quantum interferometers for frequency-domain techniques such as QIRS and FD-OCT using pulsed laser excitation.

The rest of the paper is organized as follows. In Sec. II, we propose a theoretical framework for a pulsed pump-excited nonlinear quantum interferometer using a dispersive spectrometer for detection. The experimental setup is described in Sec. III and the theoretical and experimental results are discussed in Sec. IV. In Sec. V, we summarize and conclude this work.

II. THEORETICAL ANALYSIS OF THE EFFECT OF LINEWIDTH OF PULSED LASER ON SPECTRAL DOMAIN QUANTUM INTERFEROGRAM

In this section, we derive an analytical expression for a nonlinear quantum interferogram observed using a dispersive spectrometer obtained with pulsed laser pumping. Similar to previous discussions in [15,23,25], we consider a Michelson-type nonlinear quantum interferometer, shown in Fig. 1. In this paper, we consider that pump light with an arbitrary spectrum is incident on the nonlinear crystal and generates a pair of signal-idler photons via a spontaneous parametric down-conversion (SPDC) process operating in the low-gain regime. The pump light and generated signal photons are reflected by the second dichroic mirror and are reflected back to the crystal via an end mirror. The idler photons are transmitted by the second dichroic mirror and acquire a variable phase delay due to an end mirror placed on the translation stage. The pump light passes through the crystal a second time, generating another pair of SPDC photons. Quantum interference occurs between the generation processes of these photon pairs when their optical modes are completely indistinguishable. The state of the generated photon pairs can be expressed as [23]

$$\begin{aligned}
 |\Psi\rangle = & |\text{vac}\rangle + \alpha \iint dk_s dk_i F(k_s, k_i) |1_{k_s}, 1_{k_i}\rangle \\
 & + \alpha e^{i\Delta\phi} \tau(k_i) \iint dk_s dk_i F(k_s, k_i) |1_{k_s}, 1_{k_i}\rangle \\
 & + \alpha \sqrt{1 - [\tau(k_i)]^2} \iint dk_s dk_i F(k_s, k_i) |1_{k_s}, 0_{k_i}\rangle. \quad (1)
 \end{aligned}$$

Here, $|\text{vac}\rangle$ denotes the vacuum state, $k_{s(i)}$ is the wave number of signal (idler) photons in vacuum, $|\alpha|^2$ is the conversion efficiency of the SPDC process, considered to be much lower than unity, i.e., in the low-gain regime, $|1_{k_s}, 1_{k_i}\rangle$ denotes the two-photon wave function of signal and idler photons, $\tau(k_i)$ is a phenomenological factor representing the transmission coefficient for idler photons that accounts for the reduction in visibility in the experimental setup caused by the loss of photons or mode mismatch between the first and second SPDC process, $|1_{k_s}, 0_{k_i}\rangle$ is the two-photon wave function when the idler photon is lost in the medium, $\Delta\phi$ is the relative phase delay between the pump, signal, and idler beams, and $F(k_s, k_i)$ is the normalized two-photon field amplitude. Following the discussion in Refs. [26,27], $F(k_s, k_i)$ can be expressed as the product of the phase-matching function $\psi(k_s, k_i)$ and the pump envelope amplitude $\mu(k_p)$, where $\mu(k_p) = \mu(k_s + k_i)$ using the energy conservation relation $k_p = k_s + k_i$. Therefore,

$$F(k_s, k_i) = C\psi(k_s, k_i)\mu(k_s + k_i), \quad (2)$$

where C is a normalization constant and the phase-matching function is defined as

$$\psi(k_s, k_i) = e^{i\Delta Kl} \text{sinc}\left(\frac{\Delta Kl}{2}\right), \quad (3)$$

where $\Delta K = K_p - K_s - K_i$, $K_j = n_j k_j$ ($j = \text{p,s,i}$), with n_j as the refractive index of the pump (p), signal (s), and idler (i) beam in the nonlinear crystal and l the length of the crystal. The signal photons are detected using a spectrometer with infinitely fine resolution, where the photon count rate corresponding to each signal wave number k_s is given by $P(k_s) = \langle \Psi | a_{k_s}^\dagger a_{k_s} | \Psi \rangle$. Therefore,

$$P(k_s) \propto \int dk_i |F(k_s, k_i)|^2 \{2 + \tau(k_i)e^{i\Delta\phi} + \tau^*(k_i)e^{-i\Delta\phi}\}. \quad (4)$$

We consider that the optical path length of the pump and signal arm of the interferometer is fixed at L_s . The length of the idler arm, L_i , can be tuned by moving the translation stage such that the roundtrip optical path difference between the two arms is $\delta = L_i - L_s$. The relative phase delay is $\Delta\phi = k_s L_s + k_i L_i - k_p L_s = k_i \delta$. Therefore, Eq. (4) can be expressed as

$$\begin{aligned}
 P(k_s) \propto & \int dk_i |F(k_s, k_i)|^2 \{2 + \tau(k_i)e^{ik_i\delta} + \tau^*(k_i)e^{-ik_i\delta}\} \quad (5) \\
 \propto & \int dk_i |F(k_s, k_i)|^2 \{1 + |\tau(k_i)| \cos(k_i\delta)\}. \quad (6)
 \end{aligned}$$

We first assume the case of a monochromatic cw laser source with center frequency $\omega_{p0} = ck_{p0}$, where c is the speed of light in vacuum. The pump spectrum is given by the Dirac δ function as $\mu(k_p) = \mu(k_s + k_i) = \delta(k_s + k_i - k_{p0})$. For the sake of simplicity, we rewrite $k'_i = k_{p0} - k_s$ such that the pump spectrum can be expressed as

$$\mu(k_s + k_i) = \delta(k_i - k'_i). \quad (7)$$

Therefore, the signal photon flux at k_s in a cw laser excited-nonlinear quantum interferometer is expressed as

$$P(k_s) \propto |\psi(k_s, k'_i)|^2 \{1 + |\tau(k'_i)| \cos(k'_i\delta)\}. \quad (8)$$

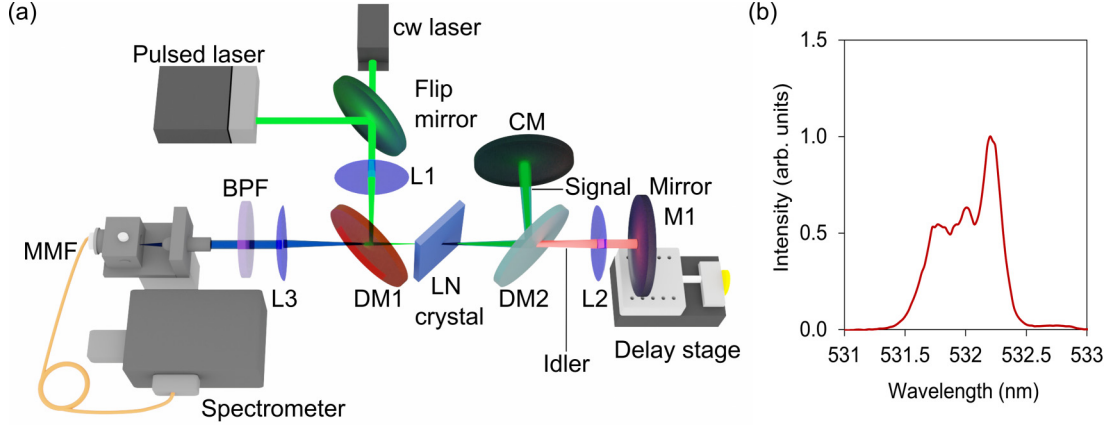


FIG. 2. (a) Schematic of experimental setup. cw laser: continuous wave laser with center wavelength 532.37 nm, average power 150 mW, linewidth < 1 MHz; pulsed laser: centroid wavelength 532 nm, average power 150 mW, pulse width 5 ps, repetition rate 80 MHz; L1: focusing lens for pump ($f = 200$ mm); L2: collimation lens for idler ($f = 100$ mm); L3: collimation lens for signal ($f = 200$ mm); DM1: long-pass dichroic mirror (edge wavelength 600 nm); LN crystal: 0.5-mm-thick, 5-mol% MgO-doped LiNbO₃ crystal with a cut angle of 76.1°; CM: concave mirror ($f = 200$ mm); DM2: long-pass dichroic mirror (edge wavelength 1000 nm), BPF: bandpass filter (center wavelength 850 nm, FWHM 50 nm); MMF: multimode fiber. (b) Spectrum of pulsed laser used in our experiment. Note that the linewidth of the cw laser is less than 1 MHz, so the spectrum is not shown.

The phase acquired by the correlated idler photons depends on the optical path difference between the two arms of the interferometer. Thus, we can observe constructive interference at $\delta = 0$, and destructive interference at k_s when $\delta \simeq \lambda'_i/2$ where $\lambda'_i = 1/k'_i$. Therefore, the visibility of the interference at a given signal wave number k_s is $V(k_s) = [P(k_s)^{\max} - P(k_s)^{\min}]/[P(k_s)^{\max} + P(k_s)^{\min}] = |\tau(k'_i)|$, where $P(k_s)^{\max(\min)}$ is the maximum (minimum) signal photon flux at k_s when the phase of the correlated idler photons is 0 (π). At a fixed delay $\delta \neq 0$, assuming k_{s1} (correlated with k'_{i1}) undergoes constructive interference, the wave number k_{s2} (correlated with k'_{i2}) will undergo destructive interference when $k'_{i2} = k'_{i1} + \pi/\delta$. Therefore, a fringelike pattern with a periodicity equal to $1/\delta$ in wave-number units is detected by the spectrometer. The quantum interference pattern for signal photons is periodically modulated with a frequency determined by δ and the pitch size of the fringe pattern decreases as δ increases. As the visibility depends only on the transmission coefficient $\tau(k'_i)$, we can observe extremely fine interference fringes with cw laser excitation according to theory.

To investigate the effect of the linewidth of a pump laser on a quantum interferogram, we now consider a pulsed laser source with an arbitrary spectrum $\mu(k_p)$ used to pump a nonlinear quantum interferometer. The finite linewidth of the pulsed laser leads to an imperfect frequency correlation between the signal and idler photon pair. Therefore, the photon flux at a particular signal wave number is computed by integrating the contribution due to all the correlated idler wave numbers k'_i satisfying the energy conservation relation $k_p = k_s + k'_i$. The photon count rate can be expressed as

$$P(k_s) \propto \int dk'_i |\psi(k_s, k'_i) \mu(k_s + k'_i)|^2 \{1 + |\tau(k'_i)| \cos(k'_i \delta)\}. \quad (9)$$

Equation (9) suggests that for $\delta = 0$, all idler photons correlated with a particular signal wavelength contribute constructively. For $\delta \simeq 0$, the phase acquired by each correlated

idler photon can be assumed to be similar. This implies that the effect of the finite linewidth of the pump laser can be ignored for the $\delta \simeq 0$ case. Thus, the visibility $V(k_s)$ around $\delta \simeq 0$ can be regarded as the intrinsic visibility for the pulsed-laser-excited nonlinear quantum interferometer. On the other hand, when the interferometric path difference δ increases, the phase $k'_i \delta$ acquired by correlated idler photons with different wave numbers varies rapidly. This results in a net reduction in the visibility at each signal wavelength. Therefore, due to the finite linewidth of the pulsed laser, the contrast of the fringe-like interference pattern also decreases as the path difference increases.

III. EXPERIMENTAL SETUP

Figure 2(a) shows a schematic of the experimental setup, consisting of a Michelson-type nonlinear quantum interferometer. The pump source can be switched between cw and pulsed laser sources using a flip mirror, allowing the effect of pump linewidth on the quantum interferogram to be investigated using a single experimental setup. We used a cw laser source (LCX-532S, Oxxius) with a 532.37 nm center wavelength, 150 mW power and < 1 MHz linewidth, and a pulsed laser source (aeroPulse PS, NKT Photonics) with a spectral centroid wavelength of 532 nm generating 5 ps pulses at an 80 MHz repetition rate with an average power of 150 mW and a full width at half maximum (FWHM) spectral linewidth of ~ 0.6 nm [spectrum shown in Fig. 2(b)].

The pump beam is focused by a lens L1 ($f = 200$ mm) on a 0.5-mm-thick, 5-mol% MgO-doped LiNbO₃ (LN) (CASTECH) crystal with a cut angle of 76.1°. The crystal is rotated such that the angle between the pump beam and the optical axis is around 68°, to generate signal (visible) and idler (near-infrared) photons with center wavelengths of 810 nm and 1.55 μm , respectively, via a type-I ($e \rightarrow \infty$) SPDC process [28]. The dichroic mirror DM2 reflects the signal and pump photons, which are then reflected back to the crystal by

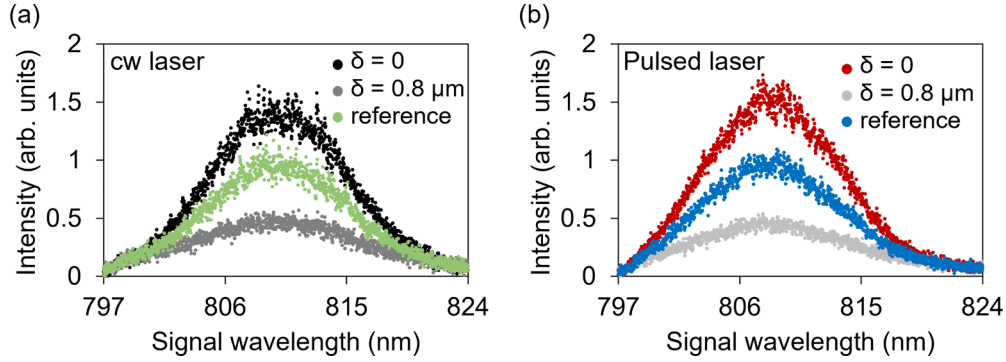


FIG. 3. Signal emission spectra obtained experimentally with (a) cw laser excitation and (b) pulsed laser excitation. The (a) green and (b) blue dots show the reference SPDC emission spectra when quantum interference is suppressed. The black and red dots show constructive interference of signal photons at an optical path difference of $\delta = 0$ nm. The dark-gray and light-gray dots show destructive interference of signal photons at $\delta = 0.8 \mu\text{m}$.

a concave mirror ($f = 200$ mm). The idler photons are transmitted by DM2, collimated by lens L2 ($f = 100$ mm), and reflected by the end mirror M1 placed on a 1-nm-resolution translational stage (FS-1020UPX, Sigma Koki).

After the second SPDC process, signal photons are transmitted via the dichroic mirror DM1 and collimated by lens L3 ($f = 200$ mm). A multimode fiber couples the interferometric signal to a visible spectrometer with a CCD array detector (SR500i+DU416A-LDC-DD, Andor, with a wavelength resolution of 0.1 nm).

IV. RESULTS AND DISCUSSION

A. Observation of quantum interferogram around zero path difference ($\delta \simeq 0 \mu\text{m}$)

Here, we confirm the observation of interference around $\delta \simeq 0 \mu\text{m}$ in our experimental setup for both cw and pulsed laser excitations using a visible-range dispersive spectrometer. First, we observed the signal emission spectrum with the cw laser source shown in Fig. 3(a). To record the reference emission spectrum of signal photons (green dots), we blocked the idler path such that no interference occurred. The center wavelength is 809.9 nm, corresponding to an idler wavelength of 1553 nm. The FWHM bandwidth of the signal emission spectrum is 12.4 ± 0.1 nm. Second, after unblocking the idler path, constructive (black dots) and destructive (gray dots) interference of almost all spectral components are observed when the optical path difference is $\delta = 0$ and $\delta = 0.8 \mu\text{m}$, respectively, with a visibility of around 49%.

Next, we switched the pump source to the pulsed laser. Figure 3(b) (blue dots) shows the reference emission spectrum of signal photons with a center wavelength of 808.4 nm and an FWHM bandwidth of 12.1 ± 0.1 nm. The corresponding plots for $\delta = 0$ and $\delta = 0.8 \mu\text{m}$ are also recorded with a visibility of around 52%. Note that the difference in center wavelengths of the generated signal spectra for the two lasers is due to the different center wavelengths of the pump sources. We conclude from Figs. 3 that spectral domain quantum interference was obtained under the same experimental conditions

for both cw and pulsed laser sources with a visibility of around 50%.

B. Evaluation of visibility $V(k_s)$ for cw laser and pulsed laser pumping

Here, we describe the procedure to extract the interference visibility $V(k_s)$ at each k_s for the interference pattern around $\delta \simeq 0$ shown in Figs. 3. In further analysis, we will compare these values with the visibility obtained at a larger path difference.

The interference visibility is extracted using the phase scanning method introduced in [23]. Figure 4(a) shows the spectral intensity of signal photons plotted as a function of the optical path difference for cw laser excitation. The interferometric signals are recorded while varying the path difference δ from 0 to 4 μm by moving the delay stage with a step size of 0.1 μm (corresponding to a change in δ of 0.2 μm).

Next, the intensity at a particular k_s varying with path difference δ is curve fitted with a sinusoidal function $y = y_0 + A \cos(k_i \delta + \phi)$, where the fitting parameter y_0 is the DC offset term, A is the amplitude, ϕ is an arbitrary phase, and k_i is fixed by energy conservation $k_p = k_s + k_i$, where k_j ($j = p, s, i$) is the wave number in vacuum for the pump (p), signal (s), and idler (i). For example, Fig. 4(b) shows the fitted curve for a center wavelength of 809.9 nm, which matches well with the experimental data. The visibility $V(k_s)$ (described in Sec. II) at each k_s is given by the ratio of the obtained fitting parameters A/y_0 .

Figure 4(c) shows the wavelength dependence of visibility obtained experimentally with cw laser excitation. The visibility at the center wavelength of 809.9 nm is $48.6 \pm 5.3\%$. The system is optimized such that the visibility is maximum around the center wavelength and the reduction in visibility around the edges can be assigned to possible mode mismatch between correlated photons due to optical aberration. To replicate the experimental visibility conditions, we use a quadratic curve fit of the wavelength-dependent visibility plot for theoretical analysis. The fitting function $V(k_s) = ak_s^2 + bk_s + c$ with fitting parameters a , b , and c is plotted as a solid orange line in Fig. 4(c).

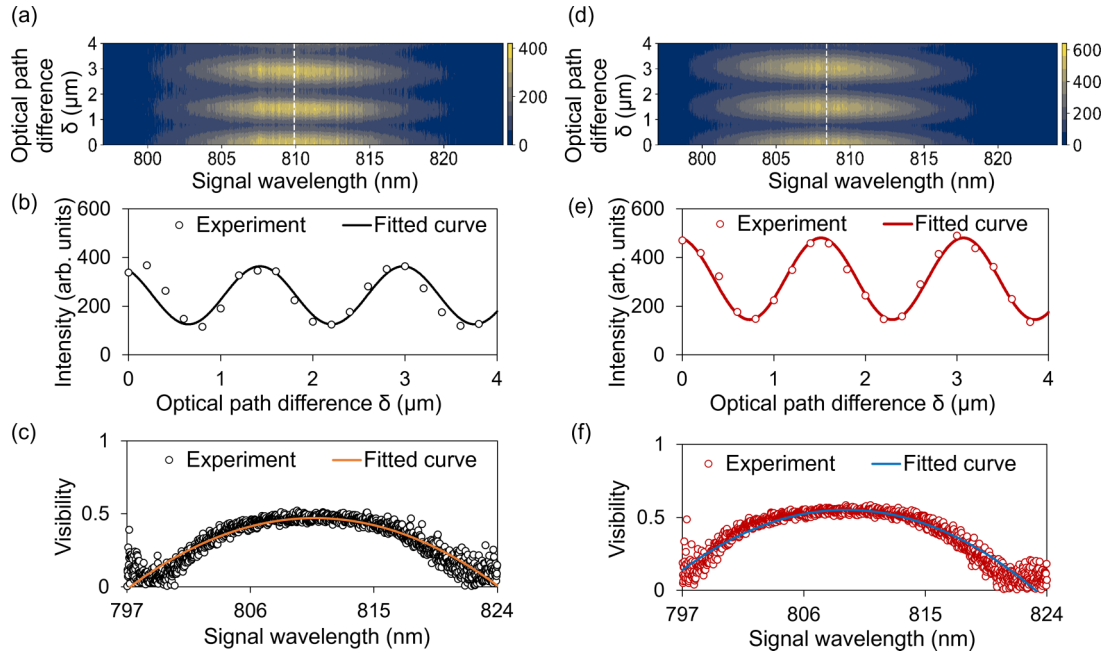


FIG. 4. (a) Spectral intensity of signal photons recorded as a function of optical path difference when $\delta \simeq 0$ with cw laser excitation. (b) Sinusoidal curve fit for intensity obtained with cw laser pumping at a center wavelength of 809.9 nm varying with optical path difference. (c) Wavelength-dependent visibility obtained with cw laser excitation evaluated using the phase scanning method. (d)–(f) The corresponding data obtained with pulsed laser excitation, with (e) showing the sinusoidal curve fit for 808.4 nm corresponding to the center wavelength of signal photons with pulsed laser excitation.

The same procedure was applied for pulsed laser excitation. Figure 4(d) shows the spectral intensity as a function of optical path difference. The sinusoidal curve fit for the experimental data for a center wavelength of 808.4 nm is shown in Fig. 4(e). In this case, k_p is fixed at the centroid wave number of the pulsed laser, and energy conservation is applied similar to the cw laser case to calculate the value of k_i . The experimentally obtained wavelength-dependent visibility for pulsed laser excitation is plotted in Fig. 4(f) (red circles) with a visibility of $53.7 \pm 2\%$ at the center wavelength. The quadratic curve fit of the visibility is shown as a solid blue line used for theoretical analysis.

It can be inferred from Figs. 4(c) and 4(f) that the visibility at the center wavelength is around 50% for both cw and pulsed laser excitations for $\delta \simeq 0$, as predicted by theory. This confirms that the results with both sources are obtained under the same experimental conditions.

C. Degradation in contrast of quantum interference fringes for optical path difference $\delta \gg 0$ using pulsed laser excitation

As discussed in Sec. II, wavelength-dependent interference occurs in the spectral domain leading to the formation of interference fringes as the path difference increases. Here, we compare theoretically and experimentally obtained interference patterns at $\delta \gg 0$ obtained by cw laser and pulsed laser pumping.

Figure 5(a) shows the theoretically computed spectrum for cw laser excitation at $\delta = 500 \mu\text{m}$ using Eq. (8), where the wavelength-dependent visibility function $V(k_s)$ (quadratic curve fit described in Sec. IV B) is substituted for $|\tau(k_i')|$. The phase-matching function is calculated using the Sellmeier

equation for a lithium niobate crystal [29] at a propagation angle of 68° , replicating the experimental conditions. The corresponding experimental data in Fig. 5(b) agree well with the theoretical prediction having a periodicity of 19.9 cm^{-1} ($\sim 1/\delta$).

Next, we plot the interferogram at $\delta = 500 \mu\text{m}$ for pulsed laser excitation. Using the actual pulsed pump spectrum $\mu(k_p)$ shown in Fig. 2(b), the visibility spectrum [solid blue curve

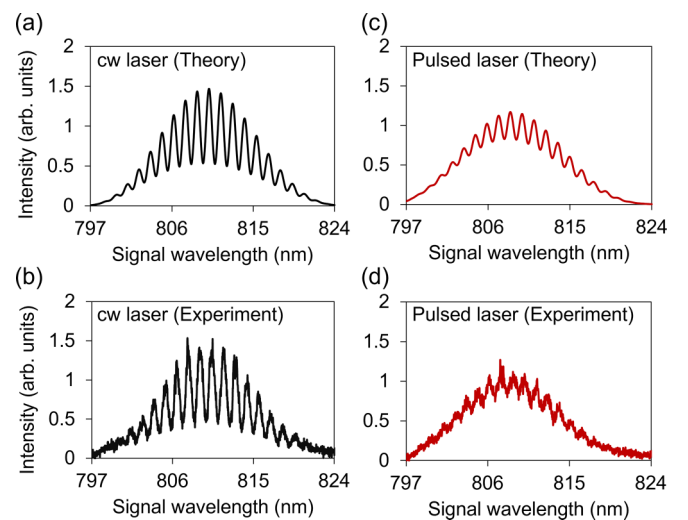


FIG. 5. (a),(b) Theoretical and experimental quantum interference patterns for signal photons at $\delta = 500 \mu\text{m}$ with cw laser excitation. (c),(d) Theoretical and experimental quantum interference patterns for signal photons at $\delta = 500 \mu\text{m}$ with pulsed laser excitation.

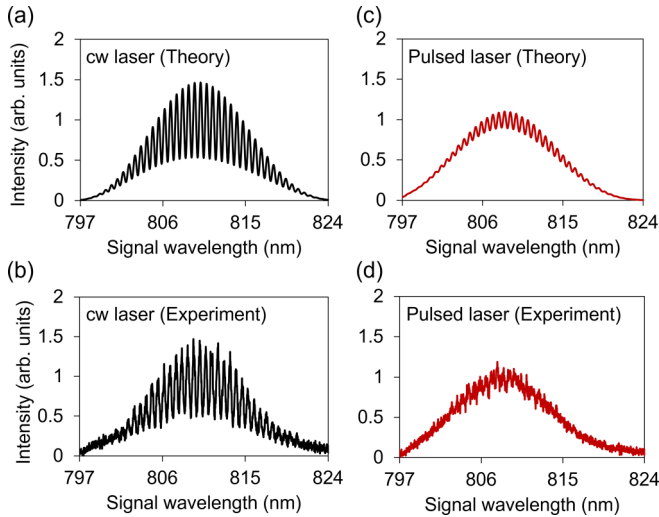


FIG. 6. (a),(b) Theoretical and experimental quantum interference patterns for signal photons at $\delta = 1000 \mu\text{m}$ with cw laser excitation. (c),(d) Theoretical and experimental quantum interference patterns for signal photons at $\delta = 1000 \mu\text{m}$ with pulsed laser excitation.

in Fig. 4(g)], and the Sellmeier equation for lithium niobate crystal, we compute the theoretical interference fringe pattern using Eq. (9), plotted in Fig. 5(c). While the periodicity of the fringes is similar to that for the cw laser pumping, a decrease in the interference contrast is observed with pulsed laser excitation. The corresponding experimental data are shown in Fig. 5(d) and also indicate reduced visibility and a periodicity of 19.68 cm^{-1} . It should also be noted that the interference spectrum with pulsed laser excitation is slightly asymmetric due to the asymmetric shape of the pump spectrum.

Similar results for $\delta = 1000 \mu\text{m}$ are shown in Figs. 6 for cw and pulsed laser excitations. The theoretical predictions for periodicity and visibility match well with the experimental data for both pump sources. Compared to the previous case, a further degradation in fringe contrast can be seen for $\delta = 1000 \mu\text{m}$ with pulsed laser pumping. In the experimental data in Fig. 6(d) with pulsed laser excitation, the fringes in the interference pattern appear almost washed out, partly due to the low signal to noise ratio of the spectral data. Thus, while the periodicity of the spectra is the same for cw and pulsed laser excitations for a particular path delay, the contrast of the fringelike interference pattern decreases as the path difference increases in the case of pulsed laser excitation.

D. Quantitative analysis of effect of pulsed laser linewidth on the visibility of interferograms

We quantitatively evaluate the reduction in visibility with pulsed laser excitation both theoretically and experimentally as the path difference is increased from 0 to $\delta \simeq 500 \mu\text{m}$ and $\delta \simeq 1000 \mu\text{m}$. For the theoretical computation, we first calculate the spectral intensity for the range of δ from 500 to 504 μm with a step size of 0.2 μm using the theory in Sec. II. The visibility values $V(k_s)$ are substituted from curve-fitted values obtained around $\delta \simeq 0$ in Fig. 4(f). The spectral intensity is plotted as a function of the path difference. For illustration,

the spectral intensity plot for $\delta \simeq 500 \mu\text{m}$ with pulsed laser excitation is shown in Fig. 7(a). The next step is to perform sinusoidal curve fitting for each signal wavelength; Fig. 7(b) shows the curve fit for a center wavelength of 808.4 nm. The corresponding experimental results are shown in Figs. 7(c) and 7(d), showing agreement with the theory.

Using a procedure similar to that described above, we obtain the wavelength dependence of visibility for the cw laser at $\delta \simeq 500 \mu\text{m}$, plotted in Fig. 8(a) (orange line). The theoretical plot agrees well with the experimental data (black dots). The experimental visibility at a center wavelength 809.9 nm is $46.2 \pm 3.4\%$. This can be compared with the pulsed laser excitation case shown in Fig. 8(b) (red dots), where the visibility at the center wavelength is reduced to $12.5 \pm 1.8\%$. The visibility predicted by the theoretical model (blue line) reproduces the experimental data well.

The wavelength dependence of visibility for $\delta \simeq 1000 \mu\text{m}$ is plotted in Fig. 8(c) for the cw laser source, showing an experimental visibility of $40.7 \pm 2.8\%$ at the center wavelength. A slight deviation in visibility is observed between the theoretical and experimental plots due to the limited resolution of the visible spectrometer. The extremely fine fringe structure can be resolved by the spectrometer for $\delta < \lambda_s^2/\Delta\lambda$, where $\lambda_s = 809.9 \text{ nm}$ and $\Delta\lambda \sim 0.1 \text{ nm}$ is the resolution of the spectrometer. However, for pulsed laser excitation, as shown in Fig. 8(d), a further decrease in the experimental visibility of the signal photons is observed, leading to $7.4 \pm 1.3\%$ at the center wavelength, which is well predicted by the theoretical model.

The variation of the visibility with increasing optical path difference is demonstrated in Fig. 9 for both cw laser and pulsed laser excitations. Using the procedure given above, we calculate the visibility at the center wavelength (809.9 and 808.4 nm for cw and pulsed laser excitation, respectively) for optical path differences varying from 0 to 1300 μm .

The visibility with the cw laser obtained experimentally (black unfilled circles) remains almost constant over 40% for δ varying from 0 to 1000 μm . This matches well with the theoretical prediction (black solid line), where there is no change in visibility for the whole range of δ from 0 to 1300 μm . The one-to-one frequency correlation between signal and idler photons results in high visibility, even when the path difference increases and, thus, high interferometric contrast is obtained.

Next, we show the visibility obtained experimentally with pulsed laser excitation. As the path difference is increased from 0 to 1000 μm , the visibility decreases from $53.7 \pm 2\%$ to $7.4 \pm 1.3\%$ (red unfilled circles). The theory (red solid line) predicts this reduction in visibility with pulsed laser pumping, and it was confirmed that the simulated visibility decreases to zero around $\delta = 2000 \mu\text{m}$. As mentioned in Sec. II, with pulsed laser pumping, the intensity of the signal photons at each k_s is computed by integrating the contribution due to the range of correlated idler photons k_i due to imperfect frequency correlation. When $\delta \sim 0$, the range of correlated idler photons is almost in phase. Therefore, the effect of pump laser linewidth can be neglected and the visibility of signal photons is higher around $\delta \sim 0$. However, as the path difference δ increases, the range of correlated k_i acquires different phases, leading to a net reduction in the visibility at each signal

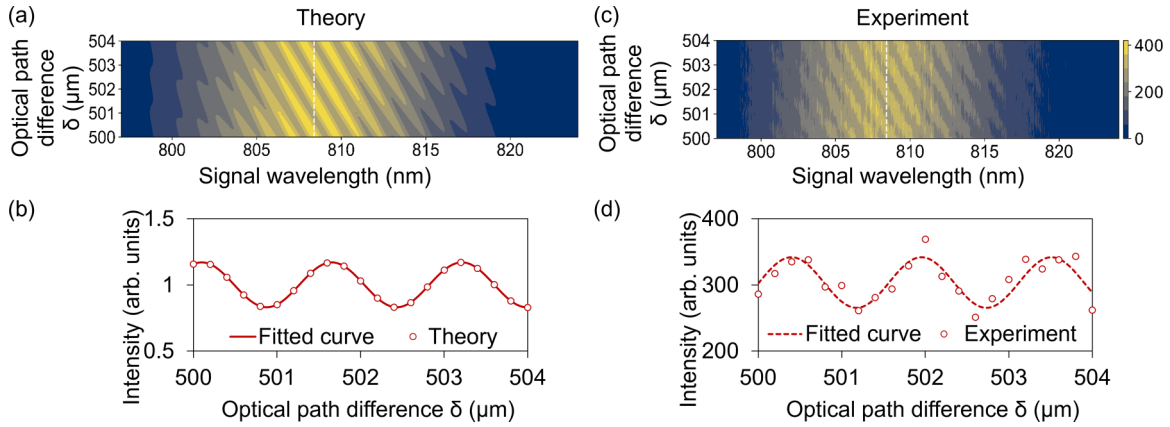


FIG. 7. (a) Spectral intensity obtained theoretically as a function of optical path difference for $\delta = 500 \mu\text{m}$ with pulsed laser excitation. (b) Sinusoidal curve fit of theoretical data shown in (a) for the center wavelength of 808.4 nm. (c) Spectral intensity as a function of optical path difference obtained experimentally. (d) Sinusoidal curve fit of experimental data shown in (c) for the center wavelength of 808.4 nm.

wavelength. Therefore, the contrast of the spectral domain interferometric fringes also decreases with increasing path difference due to the finite linewidth of the pulsed laser.

It should also be noted that the visibility decreases nonuniformly over the given range of δ (red solid line) due to the asymmetric nature of the pulsed pump spectrum. The pulsed laser used in our experiment has a multippeak spectrum [Fig. 2(b)]. When the net contribution of the side spectral components to the quantum interference pattern is in phase (out of phase) with that of the main peak component, we observe an increase (enhanced reduction) in visibility. This oscillatory effect is not observed with a pulsed laser having a symmetric Gaussian spectrum (linewidth 0.6 nm), as shown

by the reference theoretical data plotted as a gray solid line. This is because the net contribution of the side components is always in phase with that of the central pump component, which leads to a monotonic behavior.

Thus, we have shown that the spectral domain interference visibility decreases with an increase in path difference due to the finite linewidth of the pulsed laser, while it remains constant in the case of cw laser excitation. Finally, let us briefly consider the differences and similarities with classical interference of pulsed lasers. For the classical counterpart, we consider a Michelson interferometer commonly employed for characterizing the coherence length or spectral width of the pulsed lasers. First, the distinction stems from the different physical mechanisms of the two interferometers. In the

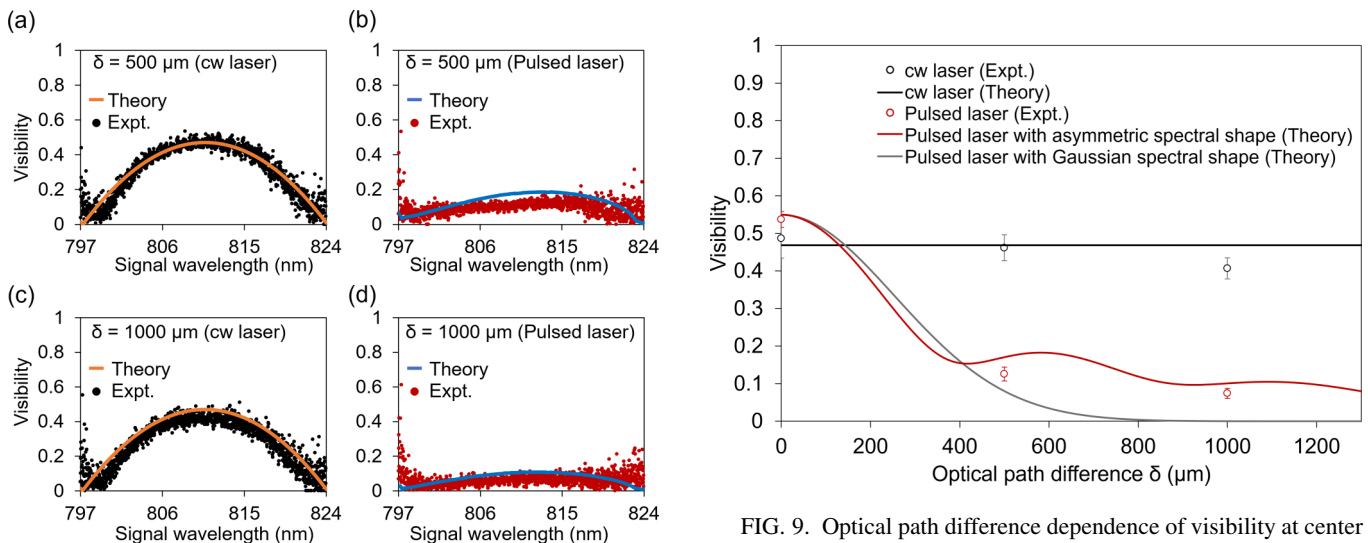


FIG. 8. Wavelength dependence of visibility evaluated at different optical path delays. (a),(b) Theoretically and experimentally obtained visibility for cw laser and pulsed laser excitation for $\delta = 500 \mu\text{m}$. (c),(d) Theoretically and experimentally obtained visibility for cw laser and pulsed laser excitation for $\delta = 1000 \mu\text{m}$. The black and red dots denote the experimental data obtained with a cw laser and pulsed excitation, respectively. The orange and blue lines denote the theoretical data for cw laser and pulsed laser excitation.

FIG. 9. Optical path difference dependence of visibility at center wavelengths of signal emission spectrum for cw and pulsed laser pumping. The black solid line shows the theoretically obtained visibility for cw laser excitation. The experimental values with cw laser pumping are plotted as black unfilled circles including error bars. The red solid line shows the visibility with the pulsed laser spectrum used in our experiment. The experimental values with pulsed laser excitation are plotted as red unfilled circles. The solid gray line shows the theoretically obtained visibility for a Gaussian pulsed laser with a spectral linewidth of 0.6 nm.

classical Michelson interferometer, interference occurs due to the phase difference between the classical electric fields. In contrast, nonlinear quantum interference occurs due to the quantum interference between the pair creation processes of signal and idler photons. Due to this quantum interference, the period of the detected interferogram of *signal photons* will have a periodicity corresponding to the wavelength of idler photons when the path length of the *idler photons* is changed. On the other hand, the similarity between the two interferometers can be found in the relation between the coherence length of the interferogram and the spectral width of the injected light. For spectral domain nonlinear quantum interferometry, which we have discussed, Eq. (9) determines the observed interferogram. When the generated photon pairs have very broad bandwidth, $\psi(k_s, k_i)$ can be approximated as nearly constant for a narrow pump spectrum $\mu(k_s + k_i)$. In this case, the coherence length of the interferogram is roughly determined by the inverse of the spectral width of the pump beam, similar to the classical counterpart. However, note that this relation cannot be valid when the SPDC emission is not broad enough.

V. CONCLUSION

We investigated the effect of the linewidth of a pulsed laser on the interference visibility of nonlinear quantum interferometry using a dispersive spectrometer. First, we derived an analytical expression for the quantum interferometric signal excited by a pulsed laser with an arbitrary spectral shape having a finite linewidth. Due to the imperfect frequency correlation between photons in a pair, the intensity at each signal wave number is determined by the contribution due to the finite range of correlated idler wave numbers. This leads to reduced visibility of quantum interference and an overall decrease in the contrast of the fringelike interference pattern as

the path difference increases. We experimentally verified the proposed theoretical framework under the same experimental conditions for a cw laser and pulsed laser to draw a comparison between them. While we observed almost constant visibility of around 46% as the path delay is increased from 0 to 500 μm for cw laser excitation, the visibility decreased from 53.7% to 12% at 500 μm for pulsed laser excitation. Considering the asymmetric nature of the pulsed laser used in our experiment, the experimental results agree with the theory.

Although the spectral properties of the pump beam are transferred to the correlation between the signal and idler photons, we have recently found that the effect of the linewidth of the pump beam strongly depends on the design of the nonlinear quantum interferometer and the detection method, which we will report elsewhere. In the case of spectral domain nonlinear interferometry studied here, we have shown that the visibility at a particular optical path difference degrades as the linewidth of the pump laser increases. We believe the detailed theoretical analysis and the rigorous experimental verification reported here are essential for deepening the understanding of nonlinear quantum interferometers. Since the pulsed laser pumping will be a useful technique for time-resolved measurements, our results are also important for applications using the spectral domain nonlinear interferometer, for example, FD-OCT and QIRS.

ACKNOWLEDGMENTS

This work is supported by the MEXT Quantum Leap Flagship Program (MEXT Q-LEAP) Grant No. JP-MXS0118067634; Cabinet Office, Government of Japan, Public/Private R&D Investment Strategic Expansion Program (PRISM); JSPS KAKENHI Grant No. 21H04444; and JST-PRESTO (Grant No. JPMJPR15P4).

-
- [1] S. Pirandola, B. R. Bardhan, T. Gehring, C. Weedbrook, and S. Lloyd, Advances in photonic quantum sensing, *Nat. Photon.* **12**, 724 (2018).
 - [2] S. Takeuchi, Recent progress in single-photon and entangled-photon generation and applications, *Jpn. J. Appl. Phys.* **53**, 030101 (2014).
 - [3] A. Alodjants, D. Tsarev, T. V. Ngo, and R.-K. Lee, Enhanced nonlinear quantum metrology with weakly coupled solitons in the presence of particle losses, *Phys. Rev. A* **105**, 012606 (2022).
 - [4] T. Nagata, R. Okamoto, J. L. O'Brien, K. Sasaki, and S. Takeuchi, Beating the standard quantum limit with four-entangled photons, *Science* **316**, 726 (2007).
 - [5] T. Ono, R. Okamoto, and S. Takeuchi, An entanglement-enhanced microscope, *Nat. Commun.* **4**, 2426 (2013).
 - [6] A. Hochrainer, M. Lahiri, M. Erhard, M. Krenn, and A. Zeilinger, Quantum indistinguishability by path identity and with undetected photons, *Rev. Mod. Phys.* **94**, 025007 (2022).
 - [7] G. B. Lemos, M. Lahiri, S. Ramelow, R. Lapkiewicz, and W. N. Plick, Quantum imaging and metrology with undetected photons: Tutorial, *J. Opt. Soc. Am. B* **39**, 2200 (2022).
 - [8] M. V. Chekhova and Z. Y. Ou, Nonlinear interferometers in quantum optics, *Adv. Opt. Photon.* **8**, 104 (2016).
 - [9] G. B. Lemos, V. Borish, G. D. Cole, S. Ramelow, R. Lapkiewicz, and A. Zeilinger, Quantum imaging with undetected photons, *Nature (London)* **512**, 409 (2014).
 - [10] A. Rogalski, Infrared detectors: Status and trends, *Prog. Quantum Electron.* **27**, 59 (2003).
 - [11] G. J. Machado, G. Frascella, J. P. Torres, and M. V. Chekhova, Optical coherence tomography with a nonlinear interferometer in the high parametric gain regime, *Appl. Phys. Lett.* **117**, 094002 (2020).
 - [12] A. Vanselow, P. Kaufmann, I. Zorin, B. Heise, H. M. Chrzanowski, and S. Ramelow, Frequency-domain optical coherence tomography with undetected mid-infrared photons, *Optica* **7**, 1729 (2020).
 - [13] A. V. Paterova, S. M. Maniam, H. Yang, G. Greci, and L. A. Krivitsky, Hyperspectral infrared microscopy with visible light, *Sci. Adv.* **6**, eabd0460 (2020).
 - [14] I. Kviatkovsky, H. M. Chrzanowski, E. G. Avery, H. Bartolomaeus, and S. Ramelow, Microscopy with undetected photons in the mid-infrared, *Sci. Adv.* **6**, eabd0264 (2020).

- [15] A. Paterova, H. Yang, C. An, D. Kalashnikov, and L. Krivitsky, Measurement of infrared optical constants with visible photons, *New J. Phys.* **20**, 043015 (2018).
- [16] C. Lindner, S. Wolf, J. Kiessling, and F. Kühnemann, Fourier transform infrared spectroscopy with visible light, *Opt. Express* **28**, 4426 (2020).
- [17] C. Lindner, J. Kunz, S. J. Herr, S. Wolf, J. Kießling, and F. Kühnemann, Nonlinear interferometer for Fourier-transform mid-infrared gas spectroscopy using near-infrared detection, *Opt. Express* **29**, 4035 (2021).
- [18] M. Arahata, Y. Mukai, T. Tashima, R. Okamoto, and S. Takeuchi, Wavelength-tunable quantum absorption spectroscopy in the broadband midinfrared region, *Phys. Rev. Appl.* **18**, 034015 (2022).
- [19] Y. Mukai, R. Okamoto, and S. Takeuchi, Quantum Fourier-transform infrared spectroscopy in the fingerprint region, *Opt. Express* **30**, 22624 (2022).
- [20] A. V. Paterova, Z. S. D. Toa, H. Yang, and L. A. Krivitsky, Broadband quantum spectroscopy at the fingerprint mid-infrared region, *ACS Photon.* **9**, 2151 (2022).
- [21] D. Y. Korystov, S. P. Kulik, and A. N. Penin, Rozhdestvenski hooks in two-photon parametric light scattering, *J. Expt. Theor. Phys. Lett.* **73**, 214 (2001).
- [22] D. A. Kalashnikov, A. V. Paterova, S. P. Kulik, and L. A. Krivitsky, Infrared spectroscopy with visible light, *Nat. Photon.* **10**, 98 (2016).
- [23] P. Kaufmann, H. M. Chrzanowski, A. Vanselow, and S. Ramelow, Mid-IR spectroscopy with NIR grating spectrometers, *Opt. Express* **30**, 5926 (2022).
- [24] R. Z. Vered, Y. Shaked, Y. Ben-Or, M. Rosenbluh, and A. Pe'er, Classical-to-quantum transition with broadband four-wave mixing, *Phys. Rev. Lett.* **114**, 063902 (2015).
- [25] Y. Mukai, M. Arahata, T. Tashima, R. Okamoto, and S. Takeuchi, Quantum Fourier-transform infrared spectroscopy for complex transmittance measurements, *Phys. Rev. Appl.* **15**, 034019 (2021).
- [26] F. Laudenbach, H. Hübel, M. Hentschel, P. Walther, and A. Poppe, Modelling parametric down-conversion yielding spectrally pure photon pairs, *Opt. Express* **24**, 2712 (2016).
- [27] T. E. Keller and M. H. Rubin, Theory of two-photon entanglement for spontaneous parametric down-conversion driven by a narrow pump pulse, *Phys. Rev. A* **56**, 1534 (1997).
- [28] M. Arahata, Y. Mukai, B. Cao, T. Tashima, R. Okamoto, and S. Takeuchi, Wavelength variable generation and detection of photon pairs in visible and mid-infrared regions via spontaneous parametric downconversion, *J. Opt. Soc. Am. B* **38**, 1934 (2021).
- [29] D. E. Zelmon, D. L. Small, and D. Jundt, Infrared corrected Sellmeier coefficients for congruently grown lithium niobate and 5 mol. % magnesium oxide-doped lithium niobate, *J. Opt. Soc. Am. B* **14**, 3319 (1997).